STIFF RAILGUNS

W.F. Weldon, J.L. Bacon, D.A. Weeks and R.C. Zowarka, Jr.

Presented at the
5th Symposium on Electromagnetic
Launch Technolohy
Eglin AFB, Florida
April 2-5, 1990

Publication No. PR-114
Center for Electromechanics
The University of Texas at Austin
Balcones Research Center
10100 Burnet Road
Austin, TX 78758-4497
(512) 471-4496

STIFF RAILGUNS

W.F. Weldon, J.L. Bacon, D.A. Weeks, and R.C. Zowarka, Jr.

Center for Electromechanics
The University of Texas at Austin
10100 Burnet Rd., Bldg. 133
Austin, TX 78758-4497

Introduction

Over the last decade the resurgence in interest in electromagnetic (EM) guns, particularly railguns, has been primarily due to their potential for accelerating projectiles to hypervelocities. This of course means that many of the most interesting railgun experiments have been performed at acceleration levels and velocities beyond those achieved in conventional guns. As a result, we have encountered and explored a number of limitations on railgun performance. In particular, this paper addresses relationships between plasma armatures, railgun structural dynamics, and rail erosion.

The experiments described were performed primarily at the Center for Electromechanics at The University of Texas at Austin (CEM-UT) between 1985 and 1988 and were supported by the U.S. Army Armament Research Development and Engineering Center (ARDEC), the Defense Advanced Research Projects Agency (DARPA), and the Strategic Defense Initiative Organization (SDIO).

Plasma Equilibrium

The plasma puffing experiments of Marshall [1] and early experiments with coaxial railguns in the Guided Electromagnetic Defense Interceptor (GEDI) program at CEM-UT have provided evidence of a mass-equilibrium condition within the plasma armature of a railgun. In Marshall's experiments, the plasma equilibrium was upset by venting the plasma through a hole in either the rail or sidewall insulator at an intermediate position along the gun. In both cases, the voltage drop across the plasma armature (muzzle voltage) quickly rose as the plasma vented and then recovered to its preventing value shortly after the armature passed the vent hole. Marshall hypothesized that the plasma mass loss through the vent was quickly regenerated from the rails and that the increase in armature voltage reflected the additional energy required to vaporize the required material. Bedford [2], upon microscopic examination of the rails from the Marshall plasma puff gun, confirmed increased rail damage down bore of the plasma vent hole and suggested it was due to the arc regenerating lost mass from the rail surface.

A set of coaxial railgun experiments were performed at CEM-UT which also support the armature mass equilibrium theory. In one experiment, a snow plow arc was initiated in the launcher by vaporizing 11 mg of aluminum. Postshot calculation of the action integral indicated that 2 mg of plasma mass entrained in the armature would match the plasma velocity obtained by inbore B-dot measurement and downrange break screens. This indicated 9 mg of vaporized fuse material was lost from the arc. After the test, aluminum deposition could be seen on the inner and outer coaxial electrodes. To further quantify the mass loss, a second experiment was designed for the coaxial launcher in which 3.2 mg of aluminum were vaporized to initiate the arc. After the experiment, the outer electrode of the barrel was plugged and filled with KOH solution. This process chemically extracted the aluminum that had been deposited on the copper barrel. This solution was then chemically analyzed and it was found that 1.1 mg of aluminum had been deposited on the wall of the outer electrode. This is a further indication of a mass-loss mechanism from the plasma armature.

The bolted-frame guns in the early GEDI program [3] were easily disassembled following a test allowing evaluation of rail and insulator materials. Initially, test shots in the GEDI program closely followed simulated performance. As higher-velocity shots were attempted, there were indications that a new performance-loss mechanism was being observed. The fourth shot of the 2-m gun showed a dramatic loss of performance which could not be explained by friction or current losses. Figure 1 shows the sidewall insulators opened and laying beside one another. Narrow pockets machined in the sidewall structural members accept different insulator samples for evaluation as bore insulation materials. In this shot, strips of quartz approximately 0.1 x 1.0 x 80 in. were epoxied into the G-10 sidewall support member. In all GEDI tests to date, the plasma has been initiated by clamping an aluminum foil in the breech of the gun. The fuse in this test was clamped 2 in. into the gun. It can be seen that there is heavy carbonization of the railgun seams from the site of fuse initiation to the point 16 in. into the gun. This is thought to be caused by the extreme thermodynamic pressure created upon vaporization of the fuse confined between the breech plug and projectile. Below the insulators is a plot of the current entering the breech of the gun when the projectile was at the respective position on the sidewall insulator shown above the trace. Also plotted is the muzzle voltage vs. position. The muzzle-voltage trace is seen to increase in the areas where a leak occurs. After the 16-in. position, the muzzle voltage falls and becomes relatively constant. It can be seen that the sidewall seams are clean during this interval until another sizable plasma leak initiates 40 in. into the gun. Once again, muzzle voltage begins to increase similarly to the increase observed in the Marshall plasma puffing experiments.

Several observations support the hypothesis above. The projectile was accelerating until it reached a position 40 in. into the gun. Up to this point the quartz glass is crushed and pieces of the quartz have actually blown out of the channel indicating high plasma pressure. After the leak site at 40 in., the sidewall shows some long cracks, but there is no pulverization of the quartz indicating a reduced pressure in this portion of the bore. The molybdenum rail coating in the second half of the gun is spotted with bubbles indicating the much greater power levels the bore was subjected to during this period of increased armature voltage.

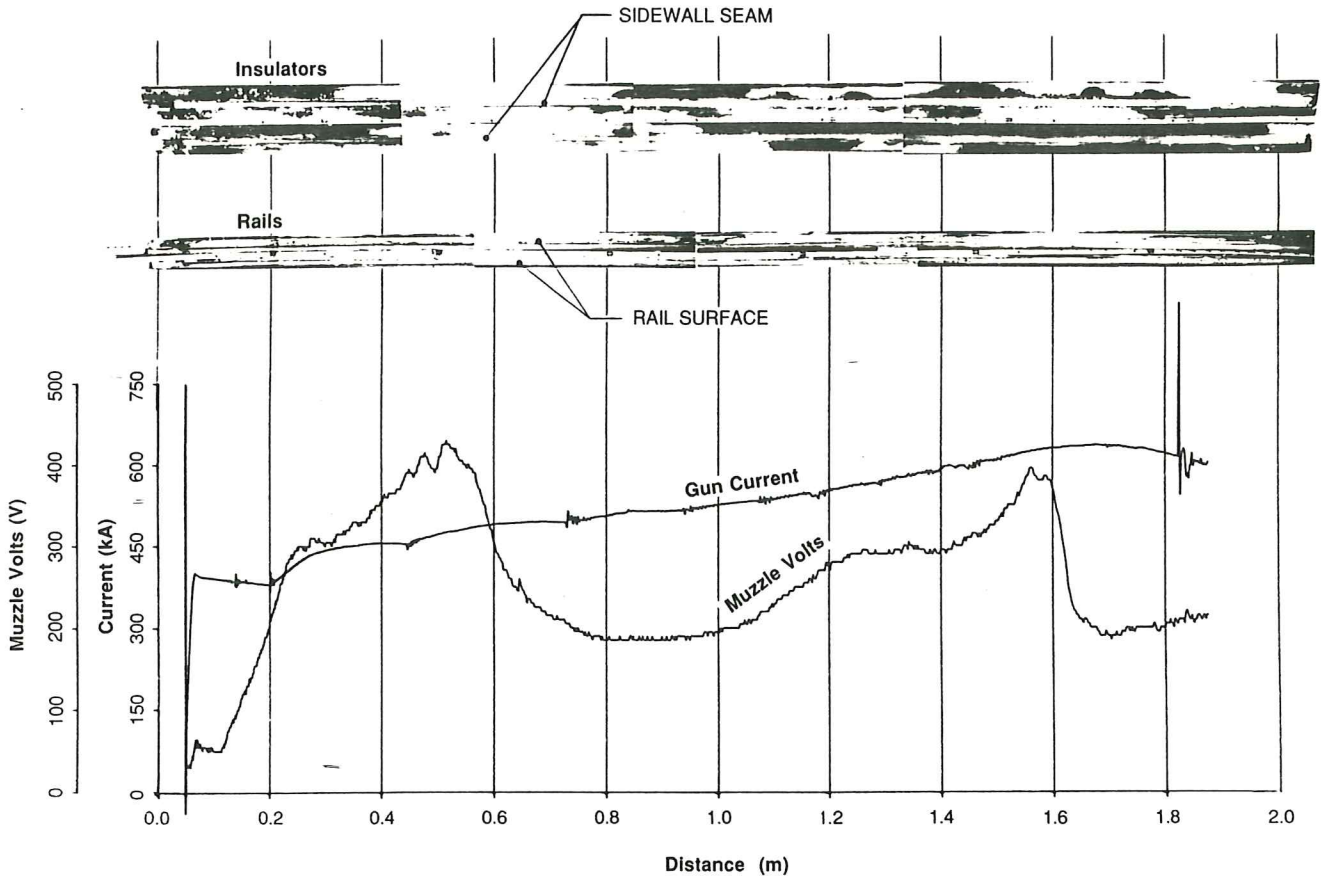

1001.0317

Figure 1. Disassembled 2 m rails and insulators with corresponding test data as a function of positon to allow direct correlation

Figure 2 is a series of histograms showing the current distribution in the gun at different time slices. These plots are generated from the rail-current-measuring B-dot probes. It can be seen that at the 40-in. position in the gun, the plasma starts to spread out and this trend continues to the end of the gun.

Predicted performance in CEM-UT bolted-frame hypervelocity railguns (fig. 3) was observed to diverge from measured performance as attempts were made to achieve velocities above 5 km/s. Increased velocity demanded increasingly higher gun currents, which in turn produced higher stresses and increased deflections in the launchers. After 2-m-long railgun test #4, it was observed that little damage occurred to the insulating quartz bore liner over the second meter, yet it was completely pulverized throughout the first meter (see fig. 1). It was also noted that in the second meter the seams between the rails and insulators, as well as the outside of the rail/insulator assembly, were covered with a black soot. The current profile during this experiment was designed to steadily increase until the projectile left the muzzle of the gun. It is thought that the total rail repulsion force on the launcher became so great after the first meter of armature travel that the gun seals were no longer effective in containing the plasma armature behind the projectile. Previously, gun current limits had been set safely below the point at which catastrophic failure of the structure would occur and consideration of bore deflections were largely ignored. After GEDI shot #4, it was suggested the gun deflection

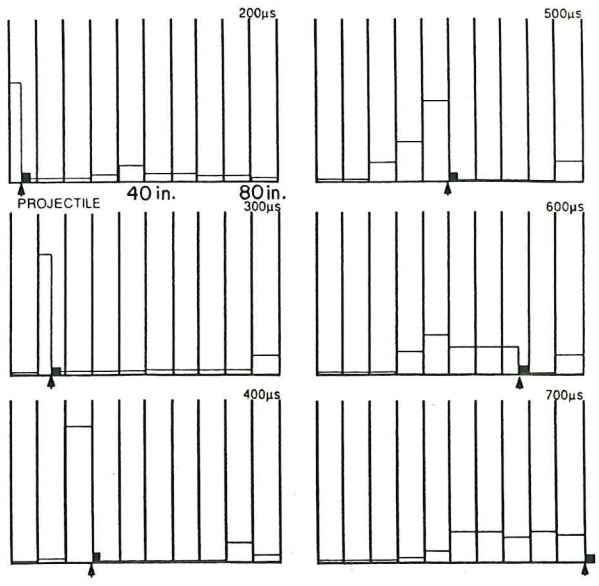

Figure 2. Histograms showing current distribution at different time slices

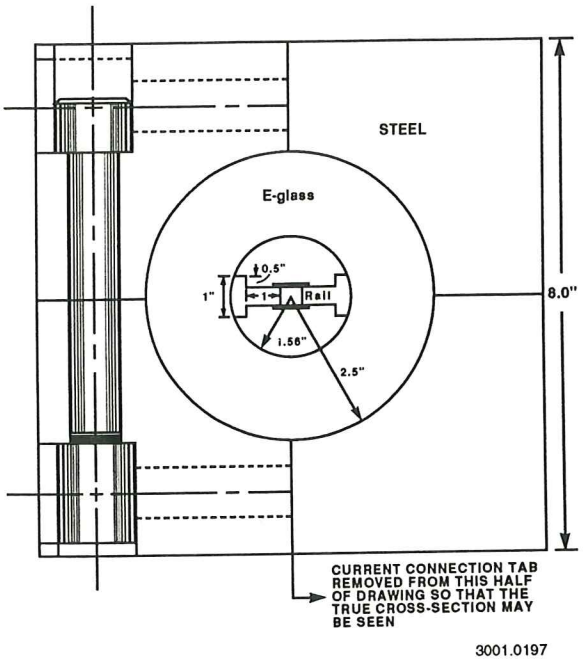

Figure 3. Bolted-frame hypervelocity railgun

based on the amplitude of the gun current at the initial initial point of plasma leakage could be used as a better criterion for determining the working current limit in a plasma armature railgun of this type. For 2-m-long railgun test #4, the B-dot probe signals in figure 4 show the armature passing 1 m at approximately 500 μs, which corresponds to a gun current of approximately 500 kA (see fig. 5). A simple analytical model for the bolted-frame railgun was formulated and the deflection as a function of applied load for a given current is shown in figure 6. The corresponding rail-to-rail deflection is 0.015 in. So it was proposed that a rail-to-rail deflection of 0.015 in. be used to determine the limiting gun current for the bolted GEDI gun.

Shots during the next few months of the program continued to show this loss mechanism until shot #24 of the 1-m railgun, which incorporated a new and much stiffer gun structure. To facilitate higher operating currents, a modification to the existing gun was designed. The gun's radial stiffness was increased by replacing the four piece bolted frame with a monolithic steel tube and radially oriented clamping discs (Ringfedder™), shown in figure 7. Rail-to-rail deflections for given gun currents are shown in figure 6. A gun current of approximately 620 kA corresponds to the previously determined limiting rail-to-rail deflection of 0.015 in.

Figure 8 presents the current vs. time data from the test of the Ringfedder™ railgun. Also shown on this plot is the actual velocity vs. time performance of the gun as derived from inbore B-dot probes and multiple-exposure flash x-ray photographs of the projectile. The maximum velocity obtained during the test was between 6 and 6.3 km/s. Also plotted is the ideal velocity derived from the action calculated from the experimental current. In the Ringfedder™ gun, a thermal kick velocity (due to vaporization of the fuse material) of approximately 600 m/s was seen on most tests. Adding this velocity to the velocity calculated from the action gives an ideal gun performance of 7,200 m/s. The experimental velocity is seen to be 83 to 88% of ideal.

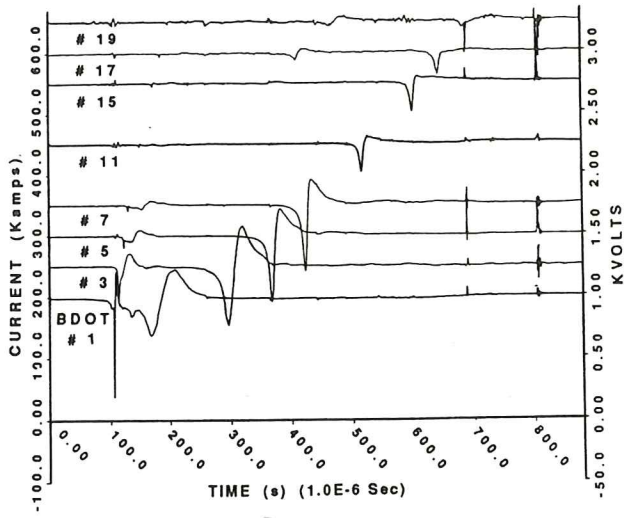

Figure 4. Axial magnetic probe signals recorded during GEDI 2-m long test #4.

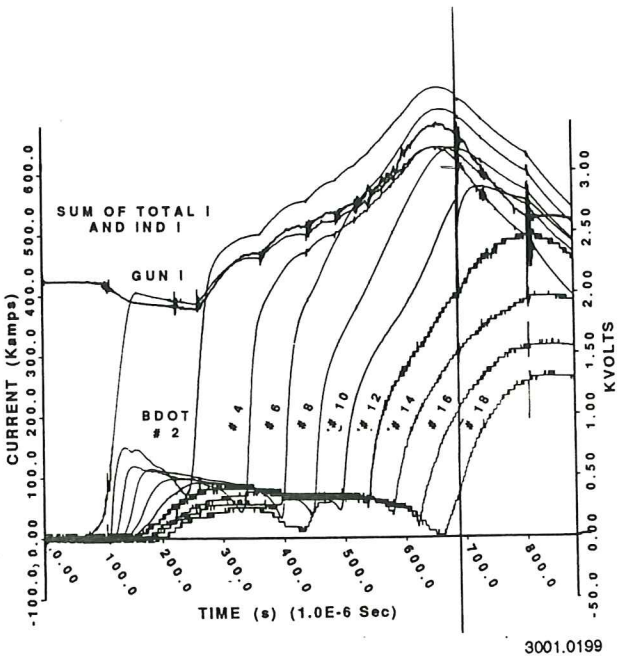

Figure 5. Gun current and radial magnetic probe signals recorded during GEDI 2-m test #4.

A next-generation railgun has been built utilizing ceramic insulators and a heavy hydraulic preload/containment structure (fig. 9). Rail-to-rail deflections for applied static loads for this type of structure are also presented in figure 6. This structure is so robust that tensile failure (catastrophic) of the ceramic components will occur (at approximately 980 kA) before rail bore deflections exceed 0.015 in.

One of the loss mechanisms suspected during this series of tests was the energy required to expand the rails against the spring constant of the frame and the additional magnetic energy stored in the gun as the rails were driven apart. To calculate this energy loss, the results of several different analytical codes were combined. A time-varying, two-dimensional, finite-element model [4] was made for the bolted-frame gun shown in figure 3. This code was used to predict the

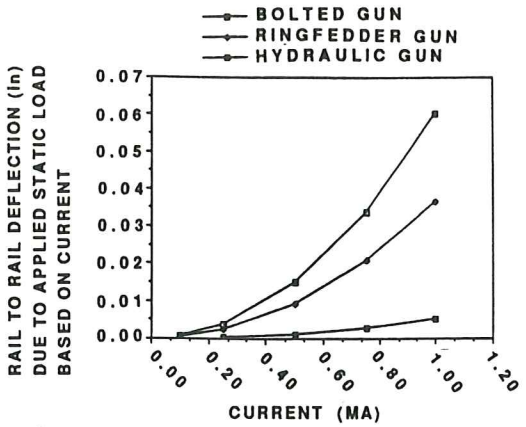

* Bolted gun and ringfedder gun deflections based on analytic methods found in Roarke and Young, "Formulas for Stress and Strain"; Hydraulic gun deflections based on finite element analysis performed by Thakore, "Dynamic Model -ing of Electromagnetic Launchers."

Figure 6. Predicted rail displacement vs. current from simple analytical model

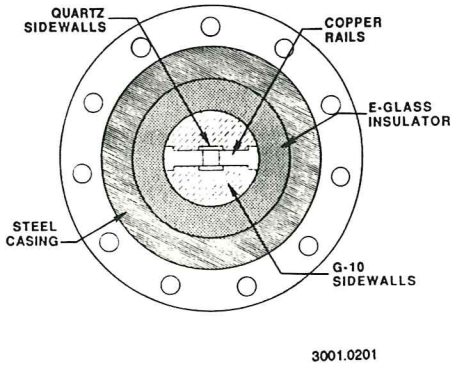

Figure 7. Cross section view of radially preloaded gun structure

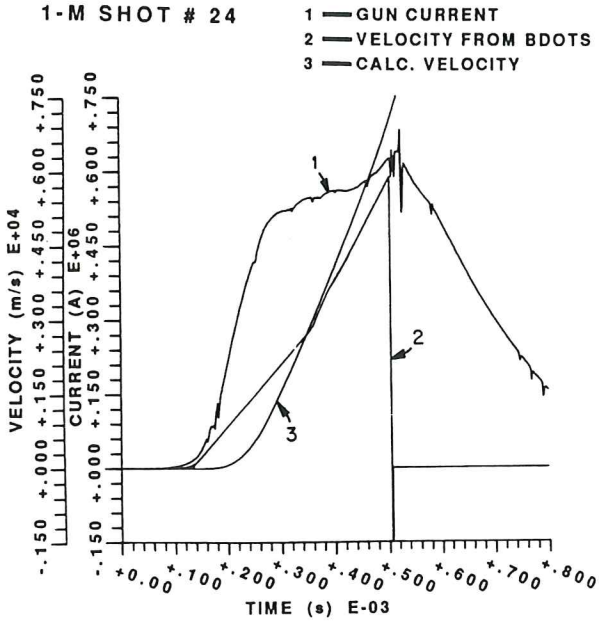

Figure 8. Measured and calculated performance from 1-m long railgun test #24

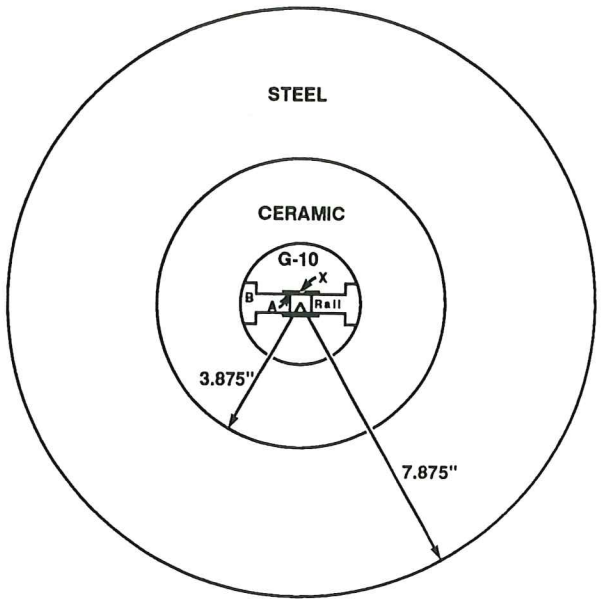

Figure 9. Railgun utilizing ceramic insulator and heavy hydraulic preload/containment structure

verify these results, Metglass™ shims were calibrated for maximum strain to failure and epoxied across the seams of the bolted frame. During an actual firing of the railgun, the failed shims indicated a displacement of 0.5 mm, which is in good agreement with the maximum displacement of 0.48 mm predicted by the transient code. The next step involved calculating the rail-to-rail separation force as a function of displacement. This was accomplished by using a code based on the method reported by Leuer[5]. Table 1 gives the rail force and displacement associated with a nominal bolted-frame railgun test. It can be seen that the strain energy is on the order of 208 J during a test in which tens of kilojoules were entering the breech of the gun. The same code that predicts rail force also allows the calculation of the inductance gradient as a function of rail displacement. The additional magnetic energy stored in the bore of the gun, due to the rail motion, was calculated to be 216 J.

Test #23 of the bolted-frame gun was used for the analysis of the strain energy stored in the railgun structure due to EM loading conditions. In that test, a 6.2-μH inductor charged to 400 kA was switched into the breech of the gun. An energy balance for that experiment was calculated from the experimental data and it was found that 95 kJ entered the breech of the gun. Of that 95 kJ, 18.6 kJ were in the kinetic energy of the 2.54-g projectile, 46 kJ were deposited in the metal vapor armature, and 17 kJ were stored in the inductance of the railgun at projectile exit. This leaves a balance of 13.4 kJ. There are methods to experimentally measure the rail resistive loss during an experiment. One such method utilizes a rail flux loop. This type of instrumentation was not available on this gun. To estimate the rail loss, a postshot simulation of the experiment was developed. The simulation breaks the rail into a large number of axial segments and defines arrays of time since projectile passage, temperature-dependent rail material properties, and internal energy for each rail segment. A simple one-dimensional diffusion model is used to predict the temperature/time history of each rail segment. This simplified model predicts that 18 kJ are deposited in the rails for the

Table 1. Rail force and displacement

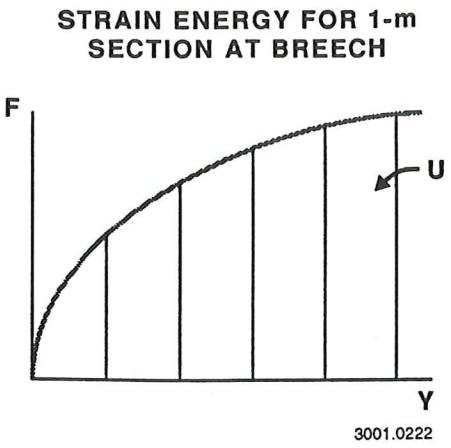

Y_N(m)	F_N(N)	ΔU(J)	U
0	0	0	0
7.793E-5	2.64E5	20.6	20.6
1.645E-4	5.60E5	35.7	64.3
1.645E-4	5.41E5	0	64.3
1.862E-4	5.22E5	11.5	75.8
2.424E-4	4.96E5	28.6	104.4

conditions of this test. This indicates that the 13.4 kJ could well be accounted for by rail heating. By comparison, it is seen that the frame strain energy is less than 1% of the two major loss terms, the armature loss and the rail heating loss.

Solid Armatures and Stiff Railguns

As stiff railguns are seen to prevent plasma leakage and improve the performance in plasma railguns, experimental evidence is accumulating that they also aid the performance of solid-armature railguns. A series of experiments have been conducted on the iron-core compulsator power supply using both Ringfedder™ railguns and bolt-frame railguns. Table 2 presents the test conditions for two such experiments. Experiment 195 was conducted with a bolt-frame gun and 196 used a Ringfedder™ or enhanced-stiffness frame. The test data is presented in fig. 10. The railgun is operated in a hot-rail configuration and the main railgun muzzle voltage is equal to the injector breech voltage, (fig. 11), up until the time that the projectile enters the main railgun. On the left side of the traces (see fig. 10) muzzle volts can be seen to drop to the voltage across the solid armature as it enters the main gun. It is also noted that the gun current was nearly identical for the two tests. Observed is that the solid armature in the stiff gun transitions later than the armature in the bolt-frame gun and the voltage of the transitioned armatures is lower in the Ringfedder™ gun for the duration of the test. The stiff structure controls rail motion and allows the armature to track the rail surface for a longer time in the gun that restricts rail motion. Because the transitioning is delayed, it can be seen that the energy deposited in the bore from the transitioned armature is less, thus reducing rail erosion and improving the efficiency of the gun. More experiments will be conducted to further quantify this effect, but preliminary findings show significant performance gains in solid armatures launched from stiff railguns.

Table 2. Compulsator test parameters

PARAMETER/RUN #	RUN #195 ACTUAL	RUN #196 ACTUAL
Compulsator Speed (rpm)	2,990	2,983
Excitation Current (A)	703	706
Open Circuit Voltage (V)	921	921
Firing Angle (% full cycle at current flow)	59.67	59.67
Firing Delay (μs)	120	144
Peak Injector Current (kA)	-159	-159
Time-at-Peak Injector Current (ms)	0.74	0.8
Peak Railgun Current (kA)	594	588
Time-at-Peak Railgun Current (ms)	3.51	3.42
Current at Armature Exit (kA)	121	118
Time at Armature Exit (ms)	5.4	5.5
Armature Velocity (m/s)	1,700	1,610

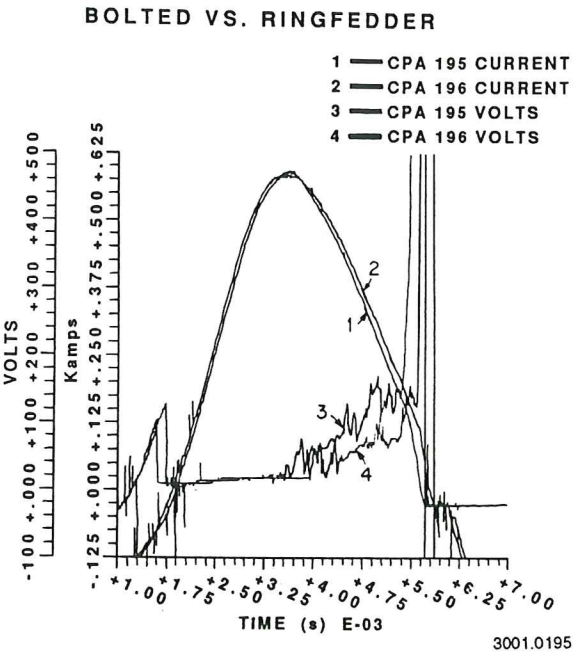

Figure 10. Performance comparison between bolted and radially clamped gun structure

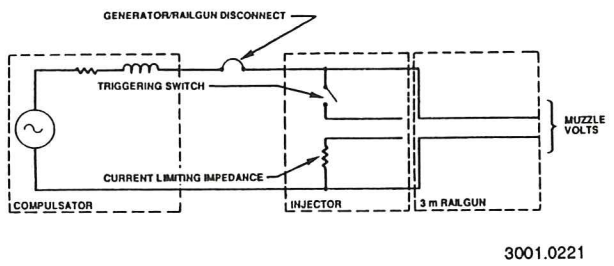

Figure 11. Iron core compulsator driven pre-injected railgun electrical circuit

Conclusions and Recommendations for Future Work

Stiff guns have been operated with both plasma and solid armatures. A performance gain was seen in the plasma railgun as stiffness was increased. A stiff gun will help to maintain the bore shape and preserve the integrity of the seam between rail and insulator under extreme asymmetric loads sustained during high-pressure operation. The hydraulically preloaded moly and ceramic gun has been fired six times at pressures as high as 87 ksi and the bore still holds roughing vacuum up to two hours after the test. The elimination of seam leakage helps control bore erosion associated with plasma reconstitution from the rail and plasma perturbation that might result in loss-initiating instabilities. Reduced rail deflection allows solid and transitioning armatures to track the bore surface. Similar to all plasma armature operation, the stiff gun seals the plasma associated with a transitioning solid armature. The efficiency of transitioning solid armatures is seen to increase in a stiff railgun. An analysis of the strain energy associated with the deflection of the railgun structure was presented and this mechanism was found to be a small fraction of the energy associated with armature loss and the rail resistive loss.

The design and scale testing of the next generation of stiff railguns is underway with the emphasis on reduced weight for field portability and space traceability requirements. Design requirements [6] and initial test results [7] are presented in other papers. Continued testing is required to further quantify the efficiency gains realized with stiff railgun structures.

References

[1] R.A. Marshall, "Plasma Puffing from a Railgun Armature," IEEE Transactions on Magnetics, vol Mag-20, no. 2, March 1984, pp 264-267.

[2] A.J. Bedford, "Rail Damage and Armature Parameters for Different Railgun Rail Materials," IEEE Transactions on Magnetics, vol Mag-20, no. 2, March 1984, pp 352-355.

[3] D.R. Peterson, D.A. Weeks, R.C. Zowarka, Jr., R.W. Cook, and W.F. Weldon, "Testing of a High Performance, Precision Bore Railgun," IEEE Transactions on Magnetics, vol Mag-22, no. 6, November 1986, pp 1662-1668.

[4] A. Thakore, "Dynamic Modeling of Electromagnetic Launchers," Masters Thesis: The University of Texas at Austin, Austin, TX, August 1988.

[5] J.A. Leuer, "Electromagnetic Modeling of Complex Railgun Geometries," IEEE Transactions on Magnetics, vol Mag-22, no. 6, November 1986, pp 1584-1589.

[6] J.H. Price, J.L. Bacon, and R.C. Zowarka, Jr., "Lightweight Large Caliber Railgun Development," presented at the 5th EML Conference, Eglin AFB, FL, April 2-5, 1990.

[7] D.A. Weeks, E.P. Fahrenthold, W.F. Weldon, and R.C. Zowarka, Jr., "Design and Testing of a Laminated Frame Railgun," presented at the 5th Meeting of the Electromagnetic Launcher Association, Auburn, AL, September 28-30, 1988.